Direct liquid injection pulsed-pressure MOCVD of large area MoS 2 on Si/SiO 2

Vincent Astié, Felipe Wasem Klein, Houssin Makhlouf, Matthieu Paillet, Jean-Roch Huntzinger, Jean-Louis Sauvajol, Ahmed Azmi Zahab, Sandrine Juillaguet, Sylvie Contreras, Damien Voiry, et al.

ARTICLE

Direct liquid injection pulsed-pressure MOCVD of large area MoS2 on Si/SiO2

Received 00th January 20xx,
Accepted 00th January 20xx

DOI: 10.1039/x0xx00000x

Vincent Astié,*[a] Felipe Wasem-Klein,[b] Houssin Makhlouf,[b] Matthieu Paillet,[b] Jean-Roch Huntzinger,[b] Jean-Louis Sauvajol,[b] Ahmed-Azmi Zahab,[b] Sandrine Juillaguet,[b] Sylvie Contreras,[b] Damien Voiry,[c] Périne Landois[b] and Jean-Manuel Decams[a]

Large-scale, high-quality growth of transition metal dichalcogenides (TMD) of controlled thicknesses is paramount for many applications in opto- and microelectronics. This paper describes the direct growth of well-controlled large area molybdenum disulfide (MoS_2) on Si/SiO_2 substrates by direct liquid injection pulsed-pressure metal-organic chemical vapor deposition (DLI-PP-MOCVD) using low-toxicity precursors. It is shown that control of the deposited thickness can be achieved by carefully tuning the amount of molybdenum precursor evaporated and that continuous layers are routinely obtained. Homogeneity and reproducibility have also been examined, as well as the average size of the grains. When targeting monolayer thickness, the MoS_2 showed near stoichiometry (S/Mo=1.93-1.95), low roughness and high photoluminescence (PL) quantum yield, equivalent to exfoliated monolayers and CVD MoS_2 grown on the same substrates.

Introduction

The Transition Metal Dichalcogenides (TMDs) have recently attracted considerable attention from both academia and industry due to a number of remarkable properties, including high on/off current ratio [1], tunable bandgap [2][3] and high flexibility [4][5]. Particularly, the properties of a selection of TMDs are drastically changed when their thickness is reduced to a monolayer [3][6]. A monolayer of TMD is composed of a hexagonally-packed lattice plane of a transition metal (e.g. Mo, W, Ti) sandwiched between two layers of close-packed chalcogen atoms (e.g. S, Se). In this family, molybdenum disulfide, MoS_2, is of particular interest in optoelectronic applications due to its transition to a direct bandgap semiconductor with very high photoluminescence quantum yield when thinned down to a monolayer [6]. A number of devices have already been presented in the literature with most of the material originating from top-down approaches such as mechanical or chemical exfoliation and transfer to a host substrate [2][4][7]. While this method generates excellent proof of concept devices, it also presents major drawbacks such as irreproducibility and limited spatial area, hindering its transfer to larger scales. Therefore, numerous bottom-up approaches have been developed for the deposition of MoS_2. For example, Chemical Solution Deposition (CSD) were developed using a large variety of sulfur and molybdenum molecules [8][9], molecular beam epitaxy (MBE) [10][11], chemical vapor deposition (CVD) [1][12], metal-organic chemical vapor deposition (MOCVD) [13], including direct liquid injection (DLI) MOCVD [14] and atomic layer deposition (ALD) [15][16][17] have been tested with a number of different precursors: MoO_3 [1][12], $MoCl_5$ [10] or organometallics such as molybdenum hexacarbonyl $Mo(CO)_6$ [10][13][14][18][19], as molybdenum source, and elemental sulfur S [1][12], carbon disulfide (CS_2) [14], bis(trimethylsilyl)sulfide (HMDST) [17], dimethyl disulfide (DMDS) [19], di-tert-butyl-sulfide (DTBS) [20] and gaseous hydrogen sulfide H_2S [18] as sulfur sources. However, most of these processes are either hardly reproducible, lengthy, result in non-continuous films, present toxic hazards or result in films with large sulfur vacancies, which then leads to degraded performances [17][21]. For future industrial applications, a scalable, fast, homogeneous, and reproducible deposition process must be developed preferably with non-toxic precursors. On that regard, Direct Liquid Injection-equipped systems have already proven to be among the most versatile MOCVD tools, providing excellent control over the stoichiometry and surface morphology of a large variety of materials [22][23]. So far, few groups have used this evaporation technique in the deposition of MoS_2 [14], and the grown material consisted in separate triangle islands of up to 3 µm in lateral dimensions rather than a continuous film.

In this paper, we report the direct growth of MoS_2 films on SiO_2/Si substrates using direct-liquid injection metal-organic chemical vapor deposition (DLI-MOCVD), atomic layer deposition (DLI-ALD) and pulsed-pressure MOCVD (DLI-PP-MOCVD). The MoS_2 samples produced from the DLI-PP-MOCVD process are continuous and exhibit good structural and optical properties with an intensity of the photoluminescence response equivalent to mechanically exfoliated samples.

[a] Annealsys, 139 Rue des Walkyries, 34000 Montpellier, France.
[b] Laboratoire Charles Coulomb, Université de Montpellier, CNRS, F-34095, Montpellier, France.
[c] Institut Européen des Membranes, CNRS UMR 5635 Université de Montpellier, 34000 Montpellier, France.
† Corresponding e-mail: vastie@annealsys.com.
Electronic Supplementary Information (ESI) available. See DOI: 10.1039/x0xx00000x

Experimental

Materials and methods

All depositions were performed in a 2-inch commercially available cold-wall MOCVD reactor (MC-050, Annealsys) similar to what was reported from McCreary et al. [14]. In this reactor, the substrates are placed in a susceptor heated via infrared lamps, which grants controlled, precise, and fast heating and cooling rates. The temperature is measured in the vicinity of the substrates with a thermocouple inserted in the susceptor to ensure that even varying conditions in the chamber, the substrate surface stays at a constant temperature (see Supplementary Information). It is also equipped with two identical direct-liquid injection evaporators capable of working in both CVD and ALD settings (Figure 1a). A detailed comparison of the different DLI methods is presented in [24]. Briefly, with DLI, liquid precursors, and even solid precursors dissolved in a solvent, can be efficiently used, and evaporated to generate gaseous species with accurate flow control allowing for precise tuning of the feeding flow and the stoichiometry to promote the desired phase [24][26]. The advantages of this evaporation method in the deposition of MoS_2 are thoroughly discussed in [14].

Deposition conditions

In this work, molybdenum hexacarbonyl $Mo(CO)_6$ (98%, Strem Chemicals) and elemental sulfur S (99.999%, Acros Organics) were used without further purification as molybdenum and sulfur sources respectively, and kept at room temperature in two distinct canisters. Precursor powders were dissolved in anhydrous toluene (99.8%, Sigma-Aldrich) to create 0.001 M ($Mo(CO)_6$) and 0.002 M (S) concentrated solutions. Both precursors are cheap, air- and moisture-stable, largely available, non-toxic and both S [1][12] and $Mo(CO)_6$ [14][18][19] have already been employed in numerous MoS_2 depositions, however, to the best of our knowledge, were never used simultaneously before this work. The very low concentration used and the mildness of the precursor chosen significantly differs from previous DLI-MOCVD reports [14], moreover, using elemental sulfur not only eliminates possible carbon co-deposition originating from pyrolysis of carbon-containing sulfur precursors [13][14], but also avoids the need for special hazardous gas treatment. In fact, by mixing sulfur vapor and hydrogen gas in the chamber, we believe that hydrogen sulfide H_2S can be generated in the vicinity of the substrate at high temperature. Unfortunately, we did not yet conduct an analysis of the species present in the chamber during deposition to confirm this hypothesis.

Thermally-grown SiO_2 on Si was chosen as deposition substrate because of its compatibility for optoelectronic devices fabrication. The 4-inch wafers were cut in samples of either 1.0x1.2 cm² or 3.5x3.5 cm² to fit in the 2-inch susceptor. The SiO_2 thickness was fixed around 90 nm in order to optimize the intensities of MoS_2 Raman and photoluminescence spectra [27].

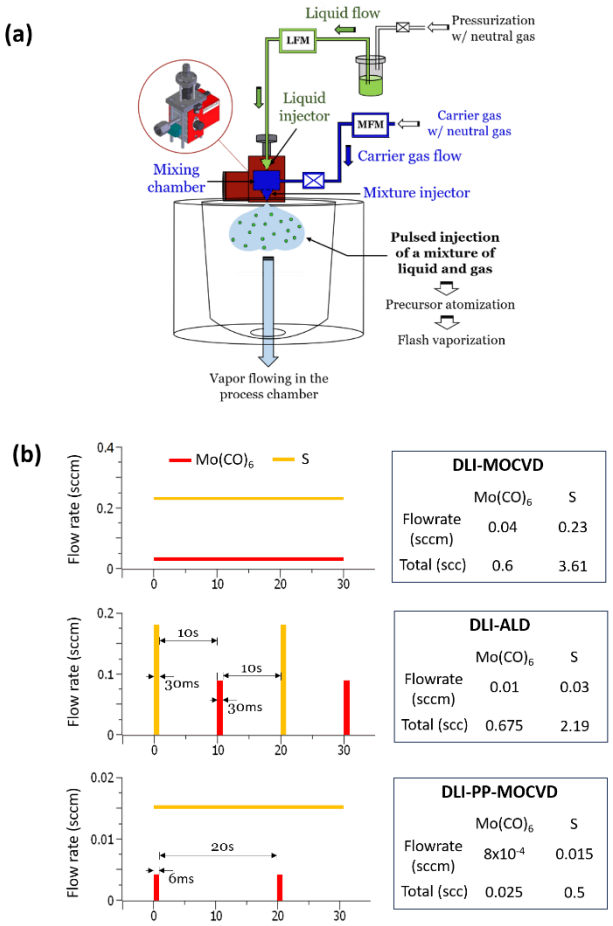

Figure 1 (a) Schematic representation of a VapBox300 showing the two stages of injections and (b) $Mo(CO)_6$ (in red) and S (in orange) injection flowrates (in sccm) during a 30s-window in each of the three process types. Average flowrates and total consumptions are indicated.

Although the use of salt, graphene-like, and alkali halide molecules has been shown to enhance adhesion and structural organization of MoS_2 films on Si/SiO_2 substrates and have been used to aid nucleation and lateral growth [1][14][28], it remains unclear how this external input affects MoS_2 properties [29][30]. Therefore, in all cases, the substrates were only cleaned in acetone, isopropanol, and deionized water under ultrasonic agitation for 10 minutes, and then, blown dry with nitrogen before being loaded in the deposition chamber.

Three types of process were investigated: DLI-Metal-Organic Chemical Vapor Deposition (DLI-MOCVD), DLI-Atomic Layer Deposition (DLI-ALD), and a mixed process, DLI-Pulsed-pressure MOCVD (DLI-PP-MOCVD). Figure 1b presents the molybdenum and sulfur precursor flow rates of a 30s-window of each of the three process types. The total amount injected where not equal, but selected to target monolayer thickness. The flowrates were calculated assuming a 100% evaporation efficiency. Note that the flowrates and total quantities used were also dramatically reduced to maximize efficiency and limit wastes. In these depositions, the average $Mo(CO)_6$ and S flowrates are 0.0008 sccm and 0.015 sccm, respectively for DLI-PP-MOCVD, far less than what is usually reported in the literature for MoS_2 depositions [10][14][18][19]. The total

process time between installation and retrieval of the samples was about 75 min in DLI-PP-MOCVD, as opposed to 32 min and 127 min for DLI-MOCVD and DLI-ALD, respectively. Both DLI-MOCVD processes were performed at 750°C in a 5% H_2:N_2 environment and the reactor pressure was kept at 5 mbar during deposition using a downstream throttle valve. The DLI-ALD processes were performed at 250°C with N_2 as sole carrier and process gas. The detailed deposition processes and conditions can be found in Supplementary Information. The use of hydrogen in MoS_2 MOCVD is said to be both beneficial and detrimental to the growth. Indeed, it should help lowering the carbon contamination induced by the metal-organic precursors but it also etches away the film as it is being deposited [31][32]. The surface morphology of the grown samples was characterized by Atomic Force Microscopy (AFM) (NanoScope V, Bruker) in tapping mode using a commercial silicon probe. Raman (resp. photoluminescence) maps and spectra were recorded at 532 nm (2.33 eV) using an Acton spectrometer fitted with a Pylon CCD detector and a 1800 grooves/mm grating (resp. 300 grooves/mm) through a x100 or x50 objective (corresponding spot diameters at half maximum around 400 nm and 800 nm, respectively). As discussed in [33], laser power was kept below 100 µW as a good compromise between minoring laser effects while yielding a signal large enough to ensure the measurements' accuracy. Optical microscopy and spectral micro-reflectometry were acquired on a Nikon LV100D with a QTH lamp, coupled with an oceanoptics USB2000+ spectrometer through a 100 µm core fiber (analyzed spot diameter between 1.0 and 1.5 µm). All the characterizations were performed at room temperature under ambient conditions.

Results and discussion

Transitioning to DLI-PP-MOCVD

Figure 2 presents the Raman and PL spectra of representative samples of each of the three process types. The samples grown from the DLI-MOCVD method, where both precursors are simultaneously and continuously injected in the chamber, were highly crystalline but consisted of nanometric grains and incorporated medium amounts of carbon, as reported by both XPS and Raman characterizations. The DLI-ALD samples, for which precursors are sequentially introduced in the chamber, were poorly crystallized and contained significant amounts of carbon. Indeed, this set of precursors is not adequate for pristine ALD MoS_2 growth and leaves residues that are then incorporated in the layers. Different precursors would have to be used to target bigger grain size and crystallinity in ALD. Even so, without post-annealing, these continuous layers can be used in applications where small grain size and high contamination levels are acceptable, in catalytic applications for example. We conducted Rapid Thermal Annealing (RTA) at 750°C for 30 seconds on a selection of ALD samples to compare with MOCVD samples (RTALD in Figure 2, see Supplementary Information). As the main issue with the MOCVD-grown samples were

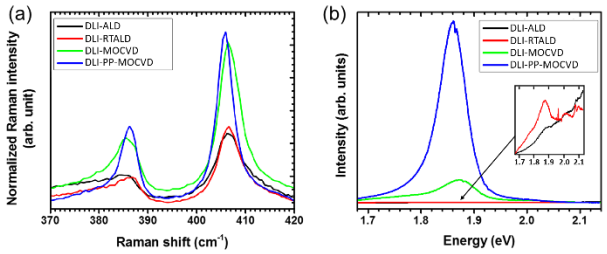

Figure 2 (a) Raman spectra normalized with respect to the Si peak intensity (not represented) and (b) photoluminescence spectra of representative samples of the DLI-ALD (black line), DLI-RTALD (red line), DLI-MOCVD (green line) and DLI-PP-MOCVD (blue line) processes.

contamination levels and low grain size, that we consider originating from the large carbon content of the molybdenum precursor and the large nucleation density respectively, we devised a mixed process between ALD and MOCVD, called DLI-Pulsed-pressure MOCVD (DLI-PP-MOCVD), where the sulfur injection is continuous to promote lateral growth and counter sulfur evaporation, and where sparse injections of $Mo(CO)_6$ (6 ms every 20 seconds, see Figure 1b) limit the nucleation density, allowing for a better control of the homogeneity and achieve bigger grains before coalescence. The change in grain size without optimization of the flow was fivefold, and tenfold after optimization. As shown in Figure 2, the optical properties were similarly vastly enhanced: while the Raman spectra are similar with a decrease in intensity for the DLI-ALD and DLI-RTALD samples due to poor crystallinity and/or small grain size, a large difference can be observed in the photoluminescence spectra of the samples, with a barely measurable emission and typical carbon markers (see inset in Figure 2b). Between the two DLI-MOCVD processes, we measured a sixfold increase of the quantum yield for the DLI-PP-MOCVD sample as compared to the DLI-MOCVD sample that could be explained by larger grain size and a lower amount of defects as targeted. Furthermore, XPS analysis confirmed that the carbon contamination of DLI-PP-MOCVD samples was limited to about 10-14 at%, and that the films exhibited good stoichiometry (1.93-1.95 S/Mo, see Figure S1 in Supplementary Information). Therefore, in the subsequent results, only DLI-PP-MOCVD samples will be discussed.

Control of growth thickness

As explained earlier, direct-liquid injection (DLI) grants total control over the molar quantities of precursor vaporized, consequently, in order to verify that the growth rate is well controlled and reproducible over different batches, height samples (S1-S8) were produced by DLI-PP-MOCVD by varying the amount of molybdenum precursor used in the process while keeping the other conditions identical. The total amount of Mo injected varies from 3.4 10^{-7} mol for sample S1 to 1.4 10^{-6} mol for sample S8.

Figure 3 shows representative AFM topography and phase images of this series of samples. As will be demonstrated in the next part with Raman spectroscopy, optical contrast, and photoluminescence, MoS_2 is present in all samples. This enables

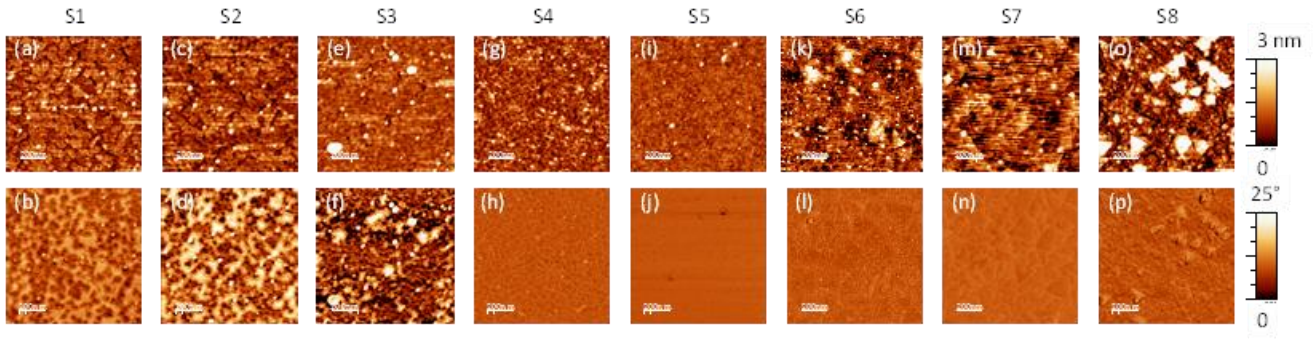

Figure 3 1x1 µm² atomic force microscopy (a, c, e, g, i, k, m, o) height and (b, d, f, h, j, l, n, p) phase images of samples S1 to S8 respectively. Colorbars are the same for all images in the line, and are shown on the right side.

the interpretation of AFM results as follows. A clear contrast in the AFM phase images of samples S1, S2 and S3 (Figure 3b, 3d and 3f, respectively) evidences the surface portions covered by MoS_2 (darker regions) and the ones uncovered (lighter regions). Conversely, the AFM phase images of samples S4, S5, S6, S7 and S8 show lower contrast suggesting that the surface is constituted of a single material, what implies that these samples are continuous, i.e. fully covered by MoS_2. On topography AFM images of samples S1 and S2, irregularly shaped domains about 50 nm wide can be identified, their height of about 0.8 nm is compatible with MoS_2 monolayer. It can also be seen that the surface becomes gradually smoother from S1 to S5 Figure 3a, 3c, 3e, 3g and 3i, respectively), while S6, S7 and S8 (Figure 3k, 3m and 3o, respectively) show larger height variations. On Figure 3l to 3p, triangular-shaped domains of about 100 nm aside are visible and some are several nanometers higher than the main surface (in particular for sample S8, about 25% of the measured heights are 1 nm or more above). This last result points out that S6, S7 and S8 are more heterogeneous in terms of MoS_2 number of layers than the other samples.

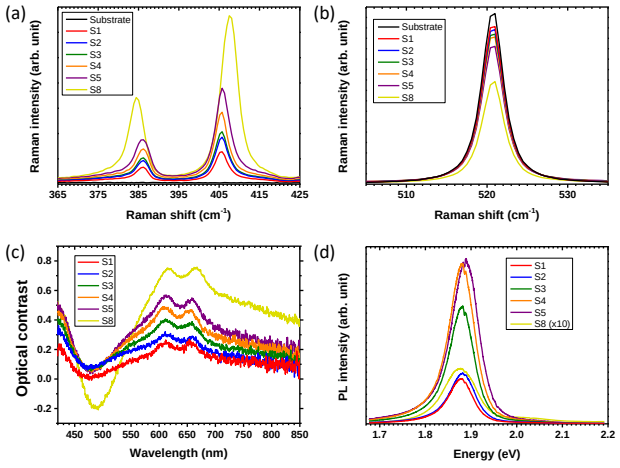

Figure 4 Optical spectroscopy characterizations of MoS_2 samples S1 to S6 synthesized by DLI-PP-MOCVD: (a) and (b) Raman spectra in the range of the (a) MoS_2 and (b) Si (underneath MoS_2 layers) modes, (c) optical contrast spectra and (d) photoluminescence spectra around 1.9 eV.

Figure 4**a**-d show the spectroscopy characterizations of samples S1-S5 and S8 which were synthesized on 96 nm SiO_2 on Si substrates. S6 and S7 are not presented because they were synthesized on substrates with a different SiO_2 thickness (87 nm) and consequently their Raman and optical contrast spectra cannot be directly compared with the others (S1-S5 and S8). In Figure 4a (resp. 4b) are displayed typical Raman spectra in the wavenumber ranges where the MoS_2 E^1_{2g} and A_{1g} modes (resp. the Si substrate T_{2g} mode around 521 cm-1) are observed The optical contrast spectra in the visible range are shown in Figure 4c and the photoluminescence (PL) spectra around 1.9 eV, i.e. in the energy range where the main peak of MoS_2 appears, are displayed on Figure 4d. For all samples, the MoS_2 Raman signature (Figure 4a), the A (around 650 nm) and B (around 600 nm) MoS_2 excitons (Figure 4c) and a strong PL signal around 1.9 eV (Figure 4d) are clearly detected. Moreover, the Raman intensity of MoS_2 A_{1g} mode (resp. Si substrate underneath MoS_2 layers T_{2g} mode) increases (resp. decreases) from samples S1 to S8 suggesting an increase of MoS_2 surface coverage and/or average thickness with the amount of Mo injected (Figure 4a(b)).

In order to extract quantitative MoS_2 thickness information, we have developed a specific Raman-based method described in details in Ref. [33]. Indeed, as shown by AFM, the samples are constituted of nanoflakes (with a lateral size of typically 50 nm, *i.e.* well below the laser spot size), with possibly a distribution of thicknesses and twist angles between adjacent layers of multilayer domains. In addition, the MoS_2 surface coverage is a priori unknown and can be incomplete. As discussed in Ref. [33], these characteristics required a reassessment of the criteria used to estimate the MoS_2 thin film average thickness. The results obtained following the approach of Ref. [33] are presented in Figure 5a. It is clearly shown that the estimated average thickness increases monotonously with the amount of Mo precursor injected during the synthesis going from 0.5 (± 0.1) up to 2.45 (± 0.25) MoS_2 layers for samples S1 to S8.

Beyond the average thickness, it was proposed to derive quantitative information about the number of layer

distributions from the analysis of ultra-low frequency (ULF) Raman spectra of DLI-PP-MOCVD MoS_2 samples [33]. ULF spectra measured on S1 to S8 samples are presented in Figure S3 (see Supplementary Information). Following the approach of [33], we plot in Figure 5b the estimated surface coverages for each number of layer (*N*) as a function of the amount of Mo precursor injected. The surface coverage is defined as the ratio between the surface covered by exactly *N* MoS_2 layers and the total surface (*N* = 0 standing for the bare substrate). In agreement with AFM (Figure 3), S4 and S5 are found very close to MoS_2 full surface coverage with about 10% and 5% of uncovered substrate remaining respectively. We can thus estimate that MoS_2 coverage is complete above 7-8.10^{-7} moles of Mo precursor injected, or above an estimated average thickness of 1.3 layers. It is also confirmed that samples S1-S3 have only about 50% of their surface coated by MoS_2. Regarding 1L MoS_2, its coverage first increases to reach a maximum around 70% for S4-S5 and then decreases. 2L is present for all samples even for those with an incomplete MoS_2 coverage. 2L coverage increases up to 1.1-1.2.10^{-6} moles of Mo precursor injected reaching a maximum of 50% for S7 and then decreases. 3L appears just above the MoS_2 full coverage threshold representing 10% of S6 and about 45% of S8. Finally, for S7 and S8 with an average thickness above 2 MoS_2 layers, 4L domains are also present. Looking back to the data presented in Figure 4 in light of this analysis, the enhancement of the optical contrast related to MoS_2 excitons A (around 660 nm/ 1.88 eV) and B (around 610 nm/ 2.03 eV) (Figure 4c) is well correlated with the increase of the average thickness from sample S1 to S5. Furthermore, the redshift of exciton A in sample S8 (to about 665 nm/ 1.86 eV) is consistent with the transition from a majority of 1 layer in S1-S5 to a majority of 2-3 layers in S8.

The behavior of the PL intensity shown in Figure 4d can also be related to the 1L MoS_2 surface coverage. Indeed, 1L MoS_2 have a higher quantum yield [4] than multilayers and their PL signal is thus expected to dominate. This point is supported by the fact that S4 and S5 have the same and highest PL intensity what correlates well with their 1L coverages being similar and the highest of the sample series despite their different 2L proportions. Overall, we find a good correlation between PL intensity and 1L coverage given the experimental errors. Extrinsic factors such as doping and defects [34] can affect PL intensity. No clear doping change between samples within this series could be evidenced by Raman scattering. Regarding defects, following the method described in [35] we estimate that the average inter-defect distance in our samples ranges from 3 to 6 nm with a slight tendency to increase with the MoS_2 thickness, *i.e.* the amount of Mo injected or synthesis duration. Overall, no clear correlation with PL intensity could be drawn, suggesting that the main parameter affecting PL intensity is indeed the 1L amount. Yet, it has been shown that DLI-PP-MOCVD MoS_2 samples with average thicknesses between 0.8 and 1.4 layers have a quasi-constant 1L coverage around 0.7 [33]. From a practical point of view, this means that samples synthesized within an interval of 5 to 8.10^{-6} moles of Mo precursor injected are showing high room temperature PL emission intensity.

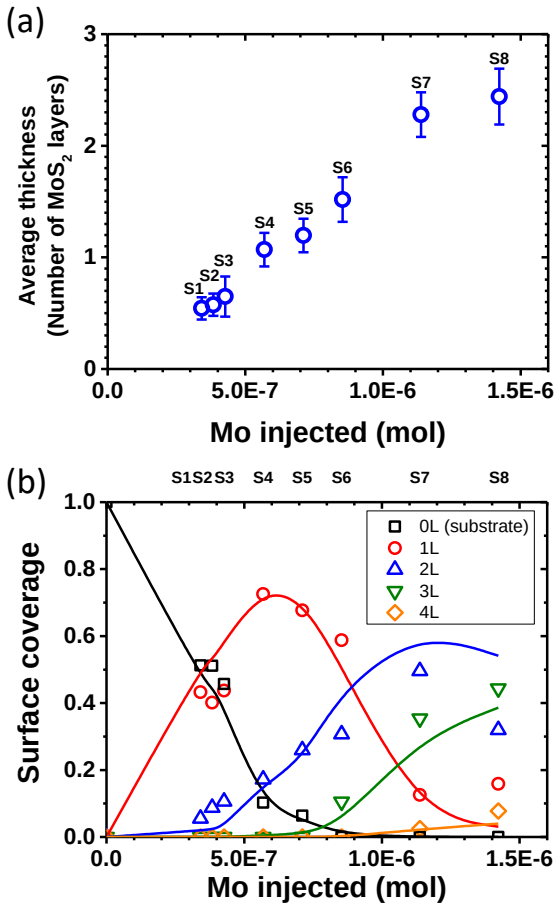

Figure 5 (a) Estimation of the deposited MoS_2 average thickness (number of layers) for samples S1 to S8 derived using the approach of Ref. [33] and plotted as a function of the total amount of Mo precursor injected during the synthesis. (b) Surface coverages of bare substrate (black open squares), 1 layer MoS_2 (red open dots), 2 layers MoS_2 (blue open up-triangles), 3 layers MoS_2 (green open down-triangles), and 4 layers MoS_2 (orange open diamonds) as function of the total amount of Mo precursor injected during the synthesis. Surface coverages are estimated from the analysis of ultra-low frequency (ULF) Raman spectra of DLI-PP-MOCVD MoS_2 samples [33]. Lines are guide to the eye.

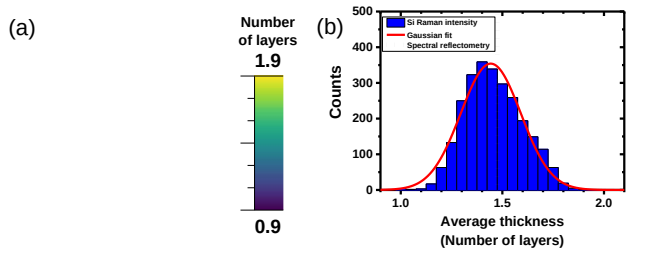

Figure 6 (a) 2 x 2 cm² map (x and y steps of 400 µm) of the Si Raman intensity converted in average thickness (number of layers) by the methodology of Ref. [33], and (b) average thickness distribution histogram extracted from the 2 x 2 cm² Raman map using Si Raman intensity (blue bars). The solid red line corresponds to a fit using a Gauss function. The average number of layers estimated using spectral reflectometry is also shown as the vertical dotted grey line.

Homogeneity

Figure 6a shows a 2x2 cm² average number of layers map (estimated using the Si 521 cm^{-1} mode Raman intensity of Si underneath MoS_2 layers, see [33] for details) measured at the center of a sample prepared by deposition on a 3.5x3.5 cm² SiO_2 on Si wafer in conditions close to S5. A thickness gradient of ≈0.2 layer/cm is observed along one of the diagonals, which is attributed to temperature and precursors concentration gradients inside the reactor, as often observed with CVD systems. In Figure 6b, we present the corresponding average thickness distributions for the 2601 points of the Raman map and the average number of layers estimated using spectral reflectometry (9 measured points equally spaced on a 1×1 cm² grid in the center of the sample). The distribution is well fitted using a Gaussian function with an average thickness of 1.4-1.5 layers and a full width at half maximum (FWHM) of ≈0.35 layers. Considering just a 1 cm² square in the center of the image, the FWHM of the distribution is of 0.2 layers, which can be considered as the heterogeneity in normal synthetic conditions. Such inhomogeneity is not surprising at this stage, since (i) the synthesis are carried out on SiO_2/Si (no epitaxy) and (ii) no attempts were yet made to control the temperature and/or precursor concentration gradients within the reactor.

Reproducibility

Reproducibility of the MoS_2 synthesis by DLI-PP-MOCVD has been tested by repeating a protocol similar to S5 (average thickness of 1.3 layers). This sample was chosen because it was observed as the thinnest one having a full surface coverage. Overall, twelve samples were produced using the same deposition conditions in four different series, each of those preceded by a full clean-up of the reactor: i) Samples 1-4; ii) Samples 5-8; iii) Samples 9-10 with a new precursor solution; iv) Samples 11-12 with the new precursor solution and after changing the position of the sample holder inside the reactor.

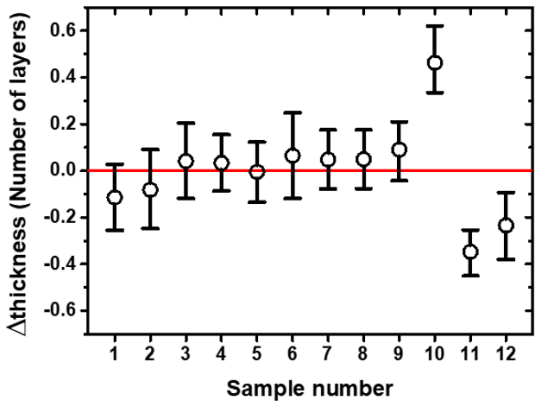

Figure 7 Difference in thickness for a series of twelve samples of MoS_2 produced by DLI in similar conditions as compared to a nominal sample with an average number of layers of 1.3. Black open dots and error bars correspond to the averages of the values determined by the 4 different measurands: optical spectral reflectometry, difference in the peak position between the A_{1g} and E^1_{2g} mode, Si Raman mode intensity and MoS_2 A_{1g} mode intensity.

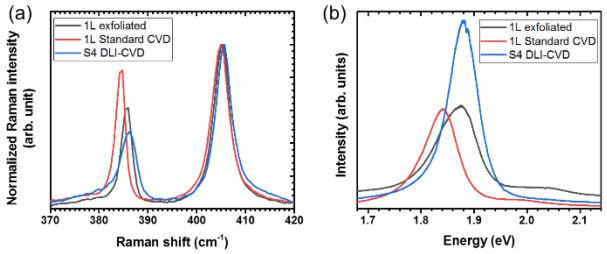

Figure 8 (a) Raman spectra normalized with respect to the A_{1g} peak intensity and (b) photoluminescence spectra of an exfoliated 1L MoS_2 (black line), a standard CVD 1L MoS_2 (red line) and the DLI-PP-MOCVD sample S4 with and average thickness of 1 (±0.15) layer (blue line).

The differences in thicknesses for these samples as compared to one of the nominal samples (Δthickness) are shown in Figure 7. For the first eight samples, made with the same reactor configuration, the average thicknesses are reliably found within 10 % of the reference sample thickness. Variation increased notably when the sample holder was moved (samples 11 and 12), which is attributed to the temperature and concentration gradients in the reaction chamber already mentioned. It is worth noting that the first sample synthesized after the reactor full clean-up (samples 1, 5, 9 and 11 here) was almost systematically found to be slightly thinner than the following ones. Thus, a first deposition after clean-up seems necessary in order to reach the reactor steady state. Overall, these results demonstrate that obtaining reproducible MoS_2 layers by the DLI method presented here is already feasible despite heterogeneities in the reactor chamber that would deserve more work to be completely solved.

Photoluminescence performance

Despite most samples consisting of a mix of 1L and 2L (and a surface coverage not always reaching 100 %), DLI-PP-MOCVD synthesized samples of average thicknesses between 0.8 and 1.4 layers (having a high and quasi-constant 1L coverage as discussed before), showed high room temperature PL emission intensity, often surpassing that of exfoliated samples or standard CVD 1L MoS_2 samples (as exemplified in Figure 8). This outperformance is in agreement with the previous DLI-MOCVD report [14] and underlines the potential for DLI-grown TMDs in optical device applications. This further underlines the role that DLI systems can play in processes where strong photoluminescence is essential.

As shown in Figure 8, in the case of the 1L standard CVD sample, the down-shift in PL energy and of the E^1_{2g} Raman mode as compared to 1L exfoliated sample are consistent with residual tensile stress [37][38]. Moreover, sulfur vacancies have also been shown to induce E^1_{2g} Raman mode downshift [36]. Interestingly, the PL peak position measured on ≈1L DLI samples is slightly upshifted compared to the exfoliated sample contrary to standard CVD samples (Figure 8b). This ties in with the changes observed in their respective Raman spectra (Figure 8a), in which an up-shift of the A_{1g} mode and an increase of the

A_{1g}/E^1_{2g} intensity ratio points toward a p-doping of the sample [37][39][40]. Furthermore, p-doping can explain the observed increased PL intensity and its up-shift [40]. The origin of the p-doping of DLI samples is not yet understood and its magnitude is found to slightly vary from one sample to another.

Conclusions

In summary, we demonstrated the deposition via Direct-liquid injection pulsed-pressure MOCVD (DLI-PP-MOCVD) of full-wafer continuous MoS_2 using $Mo(CO)_6$ and S, diluted in solvents, as precursor sources. The very low molybdenum precursor feed rate allowed for S/Mo molar injection ratio to stay modest while the stoichiometry of the near monolayer was estimated to be $MoS_{1.93\text{-}1.95}$ according to our XPS analysis (see Supplementary Information). In the case of continuous films, the depositions consisted of coalesced ≈50 nm-large grains without any visible void and with high uniformity. Reproducibility and thickness control were demonstrated with less than 10 % variation of average thickness being observed between samples made in the same conditions. On a 3.5x3.5 cm substrate, an overall thickness gradient of 0.2 layer/cm was observed. The near-monolayer samples also displayed high homogeneity in PL emission intensity and high PL yield. Thanks to the good crystalline quality and to p-doping, the PL yield is larger in near-monolayer DLI-PP-MOCVD samples than in exfoliated and CVD-grown samples. The contamination levels could be further reduced by investigating other precursors with the correct oxidation states, chosen in the wide range allowed by the DLI method. We also expect that the grain size of the coalesced film could be greatly increased by lowering even further the molar injection rate of the molybdenum source, thanks to ability of DLI to control very low flow rates.

Conflicts of interest

The authors have no conflicts to disclose.

Acknowledgements

The authors would like to thank Romain Parret for his contribution to corrections on the manuscript and valuable inputs, and the Occitania region in the frame of project DIMENSION N°2018-003267 under the program “Recherche et Société(s)”.

References

1 L. Yu, Y.-H. Lee, X. Ling, E. J. G. Santos., Y. C. Shin, Y. Lin, M. Dubey, E. Kaxiras, J. Kong, H. Wang and T. Palacios, Nano letters, 2014, 14, 3055.
2 B. W. H. Baugher, H. O. H. Churchill, Y. Yang and P. Jarillo-Herrero, Nature nanotechnology, 2014, 9, 262.
3 H. J. Conley, B. Wang, J. I. Ziegler, R. F. Haglund Jr., S. T. Pantelides and K. I. Bolotin, Nano letters, 2013, 13, 3626.
4 A. Splendiani, L. Sun, Y. Zhang, T. Li, J. Kim, C.-Y. Chim, G. Galli and F. Wang, Nano letters, 2010, 10, 1271.
5 G.-H. Lee, Y.-J. Yu, X. Cui, N. Petrone, C.-H. Lee, M. S. Choi, D.-Y. Lee, C. Lee, W. J. Yoo, K. Watanabe, T. Taniguchi, C. Nuckolls, P. Kim and J. Hone, ACS nano, 2013, 7, 7931.
6 Q. He, Z. Zeng, Z. Yin, H. Li, S. Wu, X. Huang and H. Zhang, Small, 2012, 8, 2994.
7 J.-B. Dory, O. Gauthier-Lafaye, P. Dubreuil, I. Massiot, S. Calvez and A. Mlayah, Materials Research Express, 2022, 9, 045006.
8 A. Cataldo, P. P. Tummala, C. Martella, C. S. Casari, A. Molle, and A. Lamperti, Journal of Crystal Growth,2024, 627, 127530.
9 M.-C. Chang, P.-H. Ho, M.-F. Tseng, F.-Y. Lin, C.-H. Hou, I-K. Lin, H. Wang, P.-P. Huang, C.-H. Chiang, Y.-C. Yang, I-T. Wang, H.-Y. Du, C.-Y. Wen, J.-J. Shyue, C.-W. Chen, K.-H. Chen, P.-W. Chiu, and L.-C. Chen, Nature communications, 2020, 11, 3682.
10 Y. Yu, C. Li, Y. Liu, L. Su, Y. Zhang and L. Cao, Scientific reports, 2013, 3, 1866.
11 D. Fu, X. Zhao, Y.-Y. Zhang, L. Li, H. Xu, A-R. Jang, S. I. Yoon, P. Song, S. M. Poh, T. Ren, Z. Ding, W. Fu, T. J. Shin, H. S. Shin, S. T. Pantelides, W. Zhou and K. P. Loh, Journal of the American Chemical Society, 2017, 139, 9392.
12 R. Kappera, D. Voiry, S. E. Yalcin, W. Jen, M. Acerce, S. Torrel, B. Branch, S. Lei, W. Chen, S. Najmaei, J. Lou, P. M. Ajayan, G. Gupta, A. D. Mohite and M. Chhowalla, Apl Materials, 2014, 2.
13 C. M. Schaefer, J. M. Caicedo Roque, G. Sauthier, J. Bousquet, C. Herbert, J. R. Sperling, A. Pérez-Tomás, J. Santiso, E. del Corro, Chemistry of Materials, 2021, 33, 4474.
14 K. M. McCreary, E. D. Cobas, A. T. Hanbicki, M. R. Rosenberger; H.-J. Chuang, S. V. Sivaram, V. P. Oleshko and B. T. Jonker, ACS applied materials & interfaces, 2020, 12, 9580.
15 T. Jurca, M. J. Moody, A. Henning, J. D. Emery, B. Wang, J. M. Tan, T. Lohr, L. J. Lauhon and T. J. Marks, Angewandte Chemie International Edition, 2017, 56, 4991.
16 Y. Jang, S. Yeo, H.-B.-R. Lee, H. Kim and S.-H. Kim, Applied Surface Science, 2016, 365, 160.
17 Z.-L. Tian, D.-H. Zhao, H. Liu, H. Zhu, L. Chen, Q.-Q. Sun and D. W. Zhang, ACS Applied Nano Materials, 2019, 2, 7810.
18 T. Kim, J. Mun, H. Park, D. Joung, M. Diware, C. Won, J. Park, S.-H. Jeong and S.-W. Kang, Nanotechnology, 2017, 28, 18LT01.
19 S. H. Choi, B. Stephen, J.-H. Park, J. S. Lee, S. M. Kim, W. Yang and K. K. Kim, Scientific reports, 2017, 7, 1983.
20 M. Marx, S. Nordmann, J. Knoch, C. Franzen, C. Stampfer, D. Andrzejewski, T. Kümmell, G. Bacher, M. Heuken, H. Kalisch and A. Vescan, Journal of Crystal Growth, 2017, 464, 100.
21 B. Olofinjana, G. Egharevba, B. Taleatu, O. Akinwunmi and E. O. Ajayi, Journal of Modern Physics, 2011, 2, 341.
22 A. Cherifi, M. Aouine, J.-M. Decams, C. Rocha; V. Belliere-Baca and J. M. M. Millet, Catalysis Science & Technology, 2022, 12, 3261.
23 T. Intaro, J. Hodak, P. Suwanyangyaun, R. Botta, N. Nuntawong, M. Niki, S. Kosuga, T. Watanabe, S. Koh, T. Taychatanapat and S. Sanorpim, Diamond and Related Materials, 2020, 104, 107717.
24 V. Astié, C. Millon, J.-M. Decams and A. Bartasyte, Chemical Vapor Deposition for Nanotechnology, 2018, 29.
25 P. O’Brien, N. L. Pickett and D. J. Otway, Chemical Vapor Deposition, 2002, 8, 237.
26 C. Vahlas, B. Caussat, W. L. Gladfelter, F. Senocq and E. J. Gladfelter, Recent Patents on Materials Science, 8, 108.
27 D.-H. Lien, J. S. Kang, M. Amani, K. Chen, M. Tosun, H.-P. Wang, T. Roy, M. S. Eggleston, M. C. Wu, M. Dubey, S.-C. Lee, J.-H. He and A. Javey, Nano letters, 2015, 15, 1356.
28 Y. Shi, P. Yang, S. Jiang, Z. Zhang, Y. Huan, C. Xie, M. Hong, J. Shi and Y. Zhang, Nanotechnology, 2018, 30, 034002.
29 K. Zhang, B. M. Bersch, F. Zhang, N. C. Briggs, S. Subramanian, K. Xu, M. Chubarov, K. Wang, J. O. Lerach, J. M. Redwing, S. K. Fullerton-Shirey, M. Terrones and J. A. Robinson, ACS applied materials & interfaces, 2018, 10, 40831.

30 K. Dolui, I. Rungger, C. D. Pemmaraju and S. Sanvito, Physical Review B, 2013, 88, 075420.
31 X. Li, X. Li, X. Zang, M. Zhu, Y. He, K. Wang, D. Xie and H. Zhu, Nanoscale, 2015, 7, 8398.
32 T. Chen, Y. Zhou, Y. Sheng, X. Wang, S. Zhou and J. H. Warner, ACS applied materials & interfaces, 2018, 10, 7304.
33 F. Wasem Klein, J.-R. Huntzinger, V. Astié, D. Voiry, R. Parret, H. Makhlouf, S. Juillaguet, J.-M. Decams, S. Contreras, P. Landois, A.-A. Zahab, J.-L. Sauvajol and M. Paillet, Beilstein Journal of Nanotechnology, 2024, 15, 279.
34 X. Wei, Z. Yu, F. Hu, Y. Cheng, L. Yu, X. Wang, M. Xiao, J. Wang, X. Wang and Y. Shi, Aip Advances, 2014, 4, 12.
35 S. Mignuzzi, A. J. Pollard, N. Bonini, B. Brennan, I. S. Gilmore, M. A. Pimenta, D. Richards and D. Roy, Physical Review B, 2015, 91, 195411.
36 W. M. Parkin, A. Balan, L. Liang, P. M. Das, M. Lamparski, C. H. Naylor, J. A. Rodriguez-Manzo, A. T. C. Johnson, V. Meunier and M. Drndić, ACS nano, 2016, 10, 4134.
37 Z. Melnikova-Kominkova, K. Jurkova, V. Vales, K. Drogowska-Horná, O. Frank and M. Kalbac, Physical Chemistry Chemical Physics, 2019, 21, 25700.
38 Z. Li, Y. Lv, L. Ren, J. Li, L. Kong, Y. Zeng, Q. Tao, R. Wu, H. Ma, B. Zhao, D. Wang, W. Dang, K. Chen, L. Liao, X. Duan, X. Duan and Y. Liu, Nature communications, 2020, 11, 1151.
39 M. W. Iqbal, K. Shahzad, R. Akbar and G. Hussain, Microelectronic Engineering, 2020, 219, 111152.
40 S. Kim, K. Kim, J.-U. Lee and H. Cheong, 2D Materials, 2017, 4, 045002.

